Supporting Information for "Circulation and cloud responses to patterned SST warming"

Anna Mackie[1], Michael P. Byrne[1,2], Emily K. Van de Koot[2], Andrew I.L. Williams[3]

[1]School of Earth and Environmental Sciences, University of St Andrews, St Andrews, UK

[2]Atmospheric, Oceanic and Planetary Physics, University of Oxford, Oxford, UK

[3]Program in Atmospheric and Oceanic Sciences, Princeton University, USA

Contents of this file

1. Text S1 to S3
2. Figures S1 to S9

Corresponding author: A. Mackie, School of Earth and Environmental Sciences, University of St Andrews, St Andrews, UK (arm33@st-andrews.ac.uk)

Text S1: Re-writing the zero-buoyancy plume model into pressure coordinates

The zero-buoyancy plume (ZBP) model of Singh and O'Gorman (2013) predicts, above cloud base, that the dependence of saturation moist static energy (MSE) on height is given by:

$$\frac{dh^*}{dz} = -\epsilon L_v[q^*(z) - q(z)] = -\frac{\hat{\epsilon}}{z} L_v[q^*(z) - q(z)], \tag{1}$$

where z is height, L_v is the latent heat of vaporization, and ϵ is the entrainment rate with an assumed form of $\epsilon = \hat{\epsilon}/z$ (Holloway & Neelin, 2009), where $\hat{\epsilon}$ is the entrainment parameter. The difference between the saturation specific humidity, q^*, and the specific humidity, q, is the saturation deficit.

We now transform (1) into pressure coordinates so that it can be readily applied to the pressure-level data from the simulations described in the main text. Assuming hydrostatic balance and using the ideal gas law $p = \rho R_a T_v$, where T_v is virtual temperature and R_a is the specific gas constant for dry air, we can write the vertical pressure gradient as:

$$\frac{dp}{dz} = \frac{-gp}{R_a T_v(p)}. \tag{2}$$

Integrating (2) from the surface to a pressure p yields:

$$z(p) = -(R_a/g)\ln(p/p_0)\{T_v(p)\}, \tag{3}$$

where $\{T_v(p)\} \equiv \int_{p_0}^{p}(T_v/p)dp / \int_{p_0}^{p}(1/p)dp$ is a virtual temperature inversely weighted by pressure between the surface and a given pressure level. Using (2) and (3), we can re-write (1) in pressure coordinates to obtain equation (1) from the main text:

$$\frac{dh^*}{dp} = -\frac{\hat{\epsilon}}{p\ln(p/p_0)}\frac{T_v(p)}{\{T_v(p)\}}L_v[q^*(p) - q(p)]. \tag{4}$$

Text S2: Estimation of the entrainment parameter

To estimate the entrainment parameter, $\hat{\epsilon}$, we use an optimization routine to minimize the differences between α^e_{est} and the simulated ascent fraction α across all months in the control simulation.

By design through the optimization our entrainment-adjusted estimate of ascent fraction α^e_{est} $= \alpha = 0.48$. This can be visualised in Figure 2a: the optimization routine finds the value of $\hat{\epsilon}$ which produces an α^e_{est} over the 12 months to adjust the horizontal blue line such it lies on the red line: this gives the purple horizontal line. This returns a value of $\hat{\epsilon} = 0.18$. Our optimized $\hat{\epsilon}$ is smaller than the value of 0.75 calculated by Singh and O'Gorman (2013), though differences are perhaps unsurprising given their study used a limited-domain, cloud-resolving model versus the GCM simulations with parameterized convection analyzed here.

Text S3: Testing the WTG-approximation in the instability index

We test the consistency of our results with the WTG approximation in our framework by defining an estimate of saturation MSE in the perturbation simulations: $h^{*p}_{500,est} \equiv h^{*c}_{500} + \overline{\Delta h^*_{500}}$, where p and c refer to perturbation and control simulations, respectively, and $\overline{\Delta h^*_{500}}$ is the tropical-mean change in saturation MSE at 500hPa. Note that the specific assumption invoked here is not that free-tropospheric saturation MSE is spatially uniform across the tropics, rather that changes in saturation MSE are spatially uniform (a prediction consistent with the WTG approximation). We then use $h^{*p}_{500,est}$ to calculate our entrainment-adjusted instability index, Φ^e, and find that this 'WTG-test' estimated ascent fraction is very similar to the α^e_{est} as described in Section 3.2 (Fig. S3).

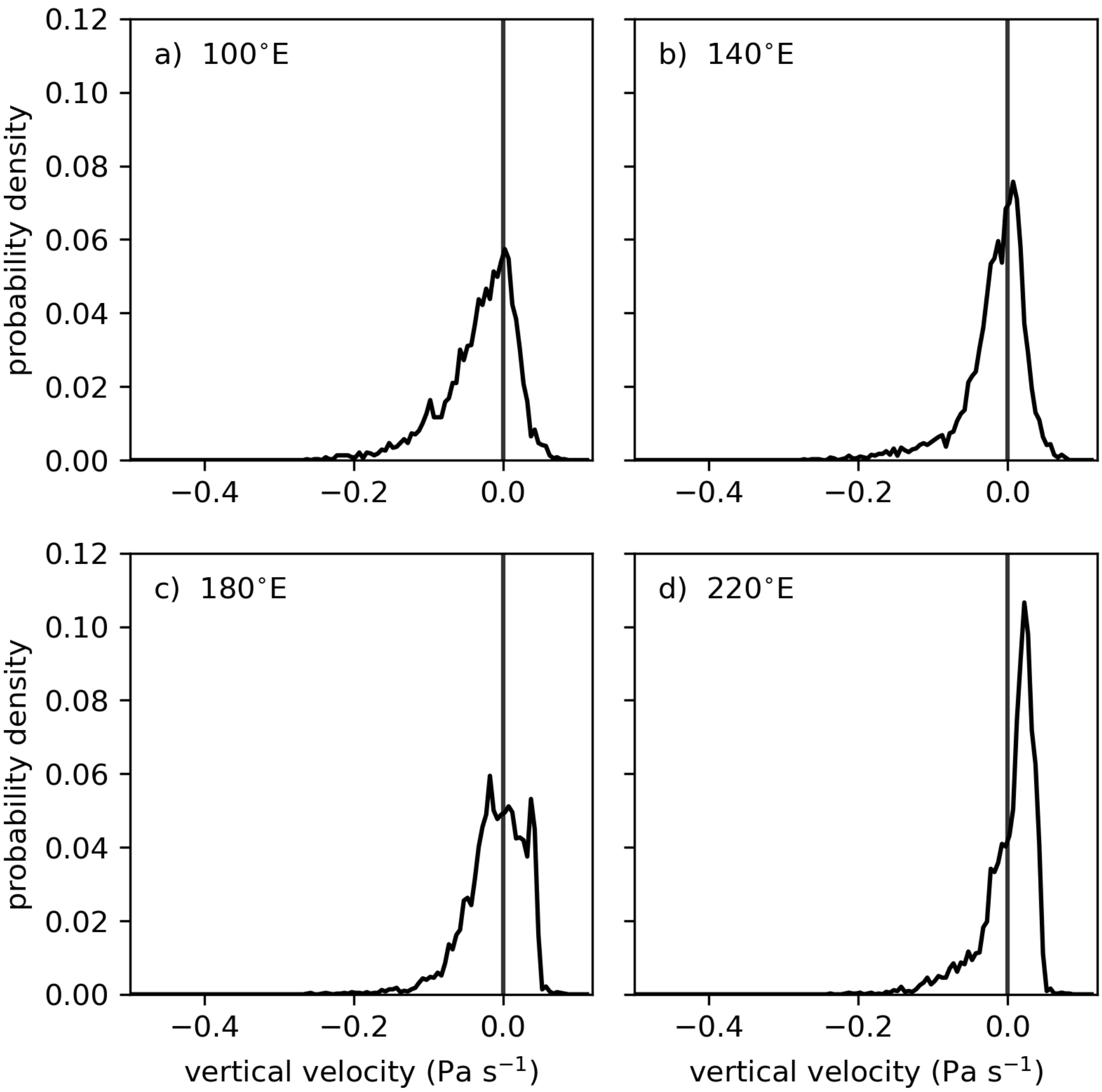

Figure S1. Probability density functions (PDFs) in the control simulation of 500 hPa vertical velocity above the SST warming patches centered at: (a) 100°E; (b) 140°E; (c) 180°E; and (d) 220 °E. Extent of the patch is defined as gridpoints with an SST change of greater than +0.4 K in the +4 K warming simulation.

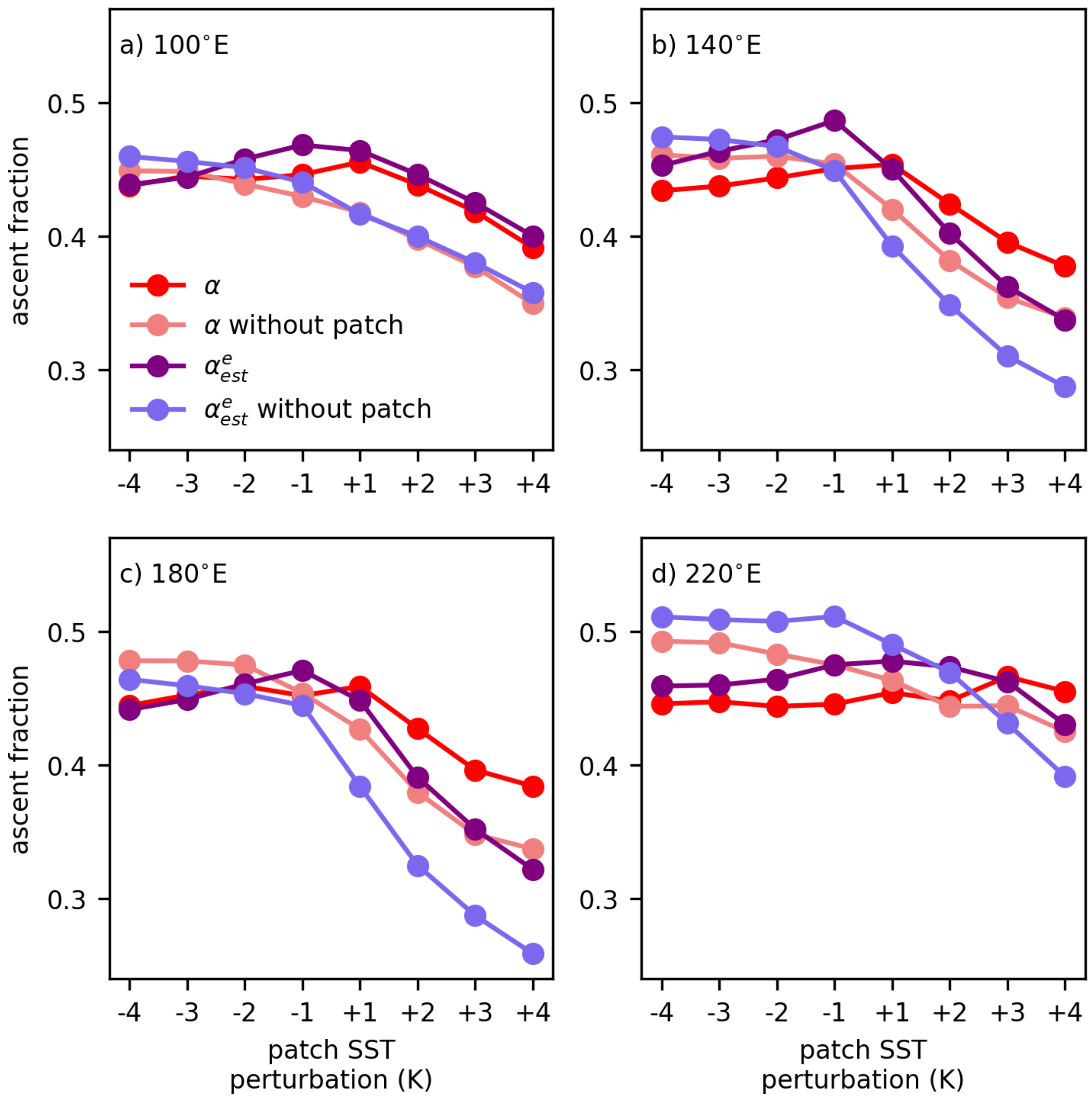

Figure S2. As for Figure 1 in the main text, but here including results for ascent fraction calculated with vertical velocity at 500 hPa (peach lines) and the entrainment-adjusted instability index (light blue lines) excluding directly warmed grid points (as defined as gridpoints with an SST change of greater than +0.4 K in the +4 K warming simulation).

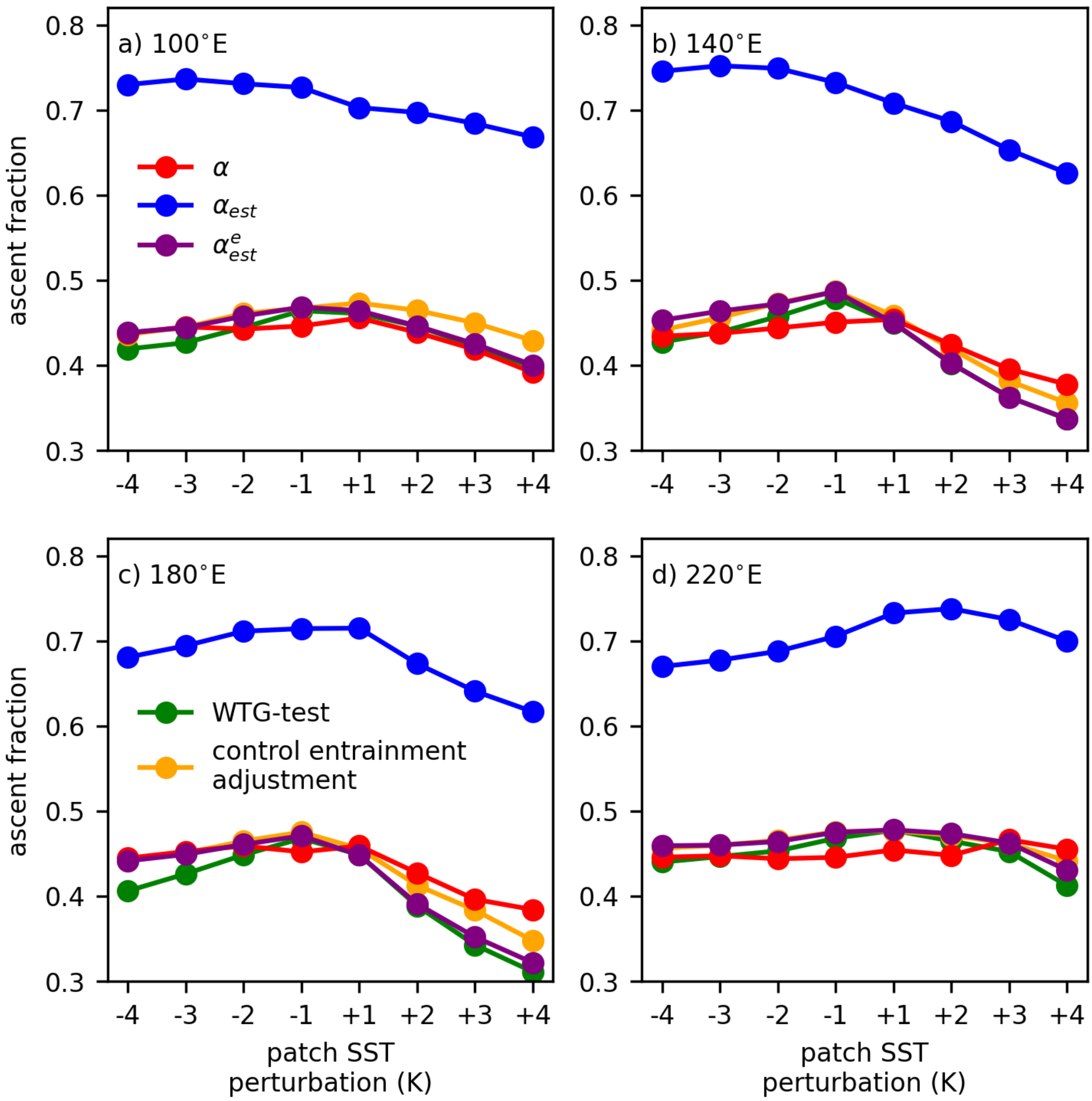

Figure S3. As for Figure 1 in the main text, but here including: the ascent fraction as estimated by instability index unadjusted for entrainment (blue lines); results testing the WTG assumption (green lines, see Text S3 for details); and results testing the effects of using $[h^{*e}]$ from the control simulation rather than from the perturbation simulation (orange lines, see Section 3.2).

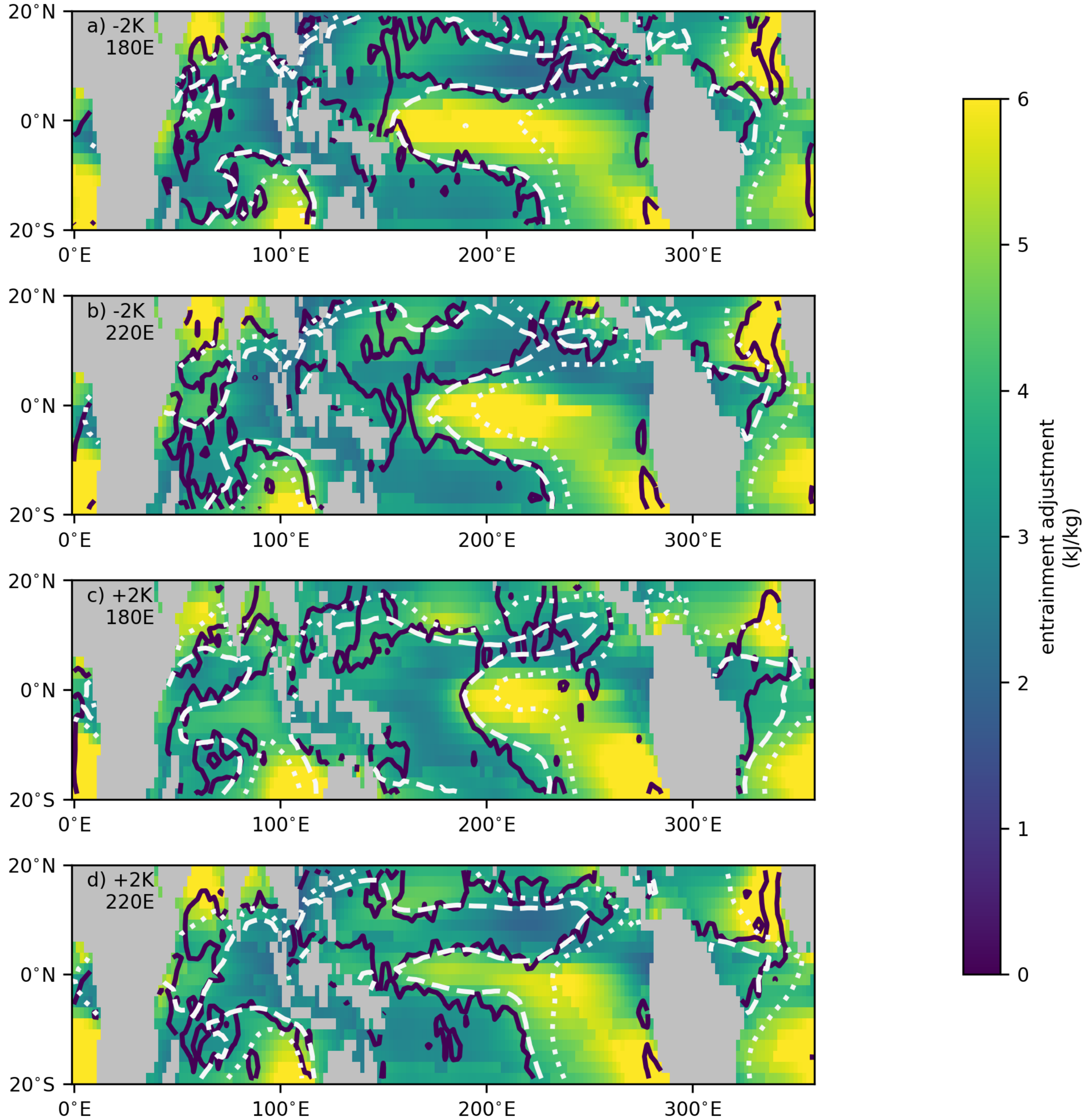

Figure S4. Entrainment-adjustment term $\hat{\epsilon}h^{*e}$ for: (a) -2 K perturbation centered at 180°E; (b) -2 K at 220°E; (c) +2 K at 180°E; and (d) +2 K at 220°E. Also included are zero contours for the unadjusted instability index Φ (dotted white) and entrainment-adjusted instability index Φ^e (dashed white) and 500 hPa vertical velocity (solid dark blue).

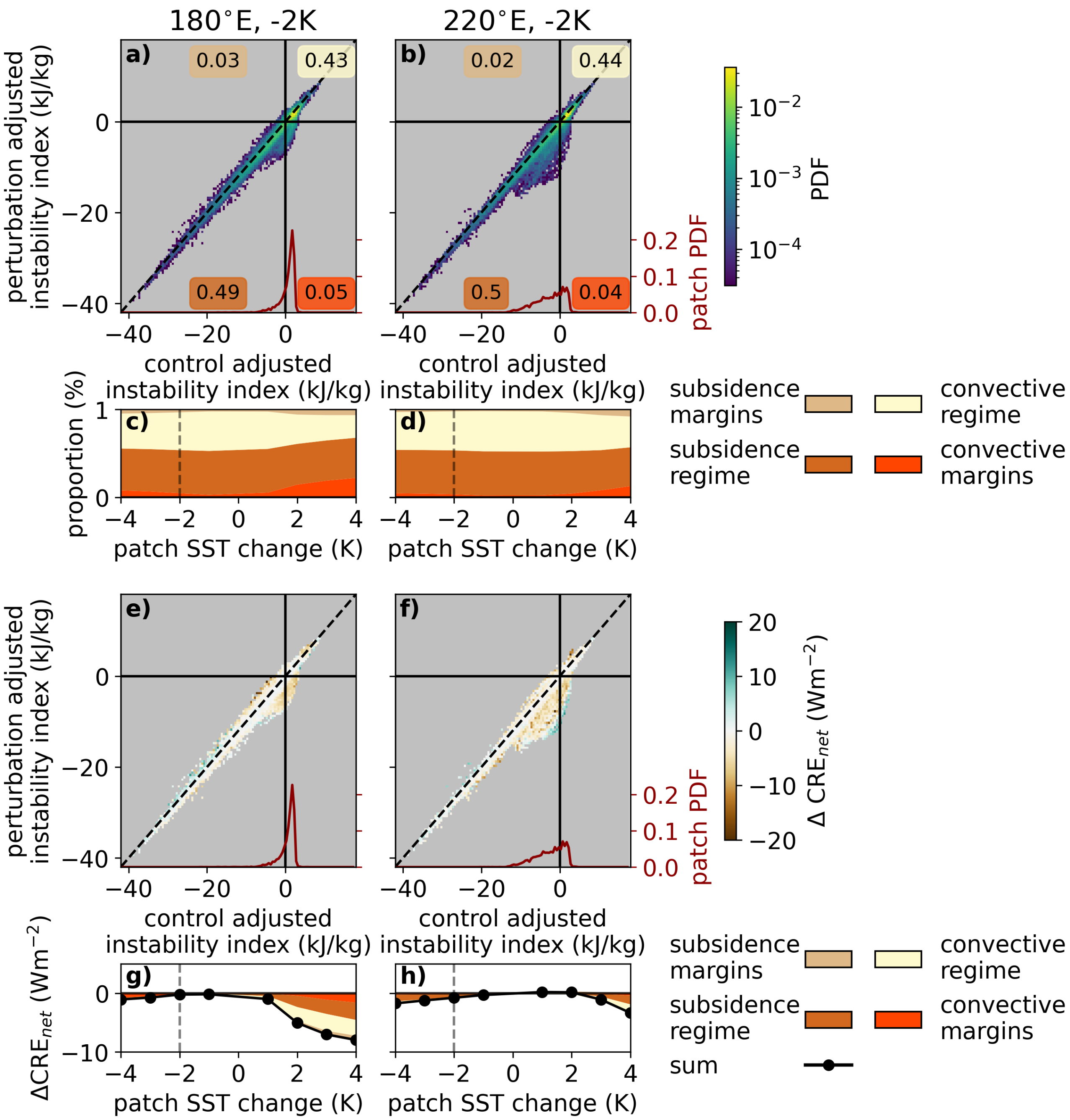

Figure S5. As for Figure 3 in the main text, but here for the -2K simulations.

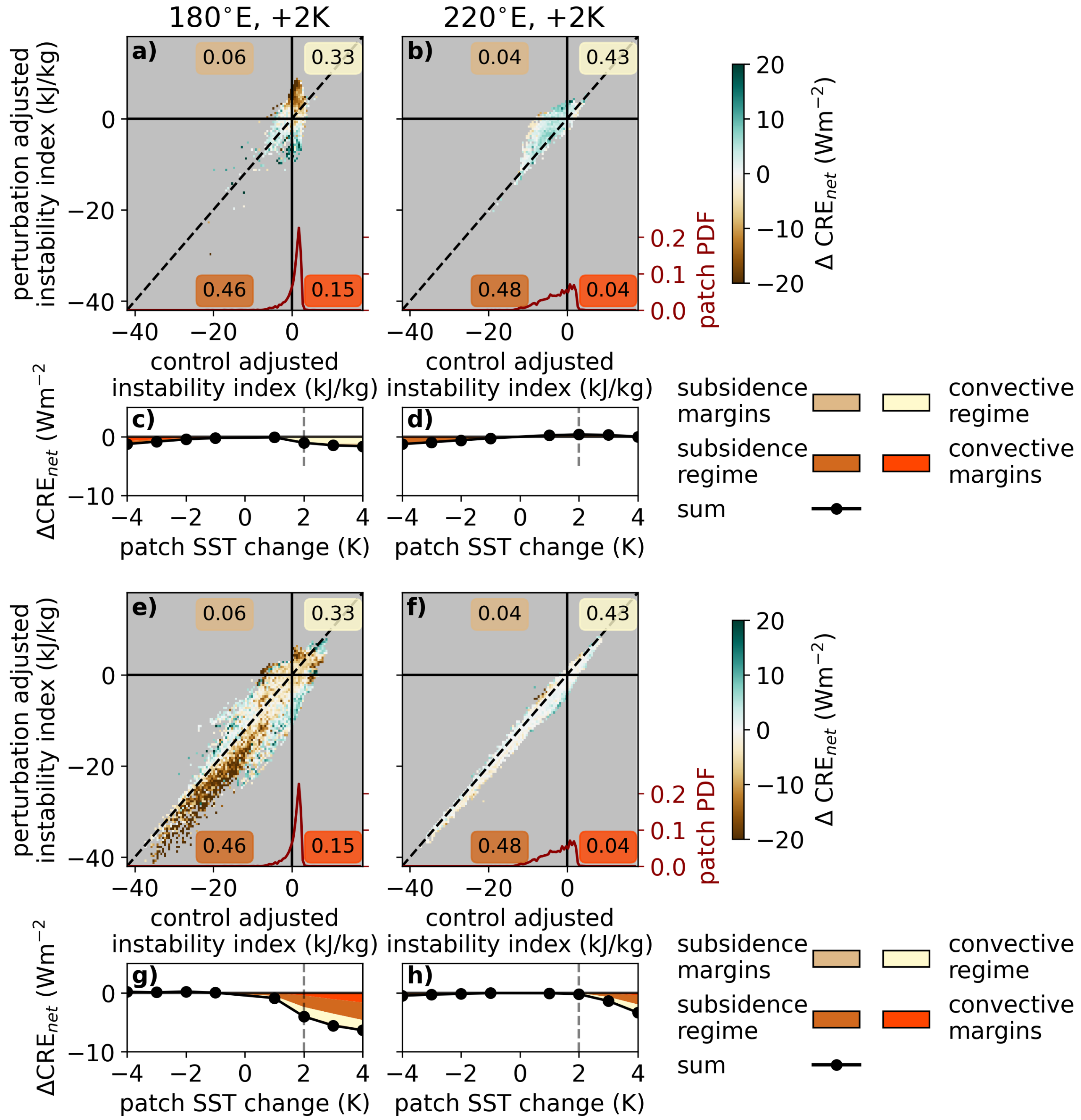

Figure S6. As for Figure 3e-h in the main text, but here showing the change in net cloud radiative effect for: (a)-(d) gridpoints which are directly warmed at the surface (i.e., fall within the SST warming patch); and (e)-(h) those which are not (i.e., fall outwith the patch). Extent of the patch is defined as gridpoints with an SST change of greater than +0.4 K in the +4 K warming simulation.

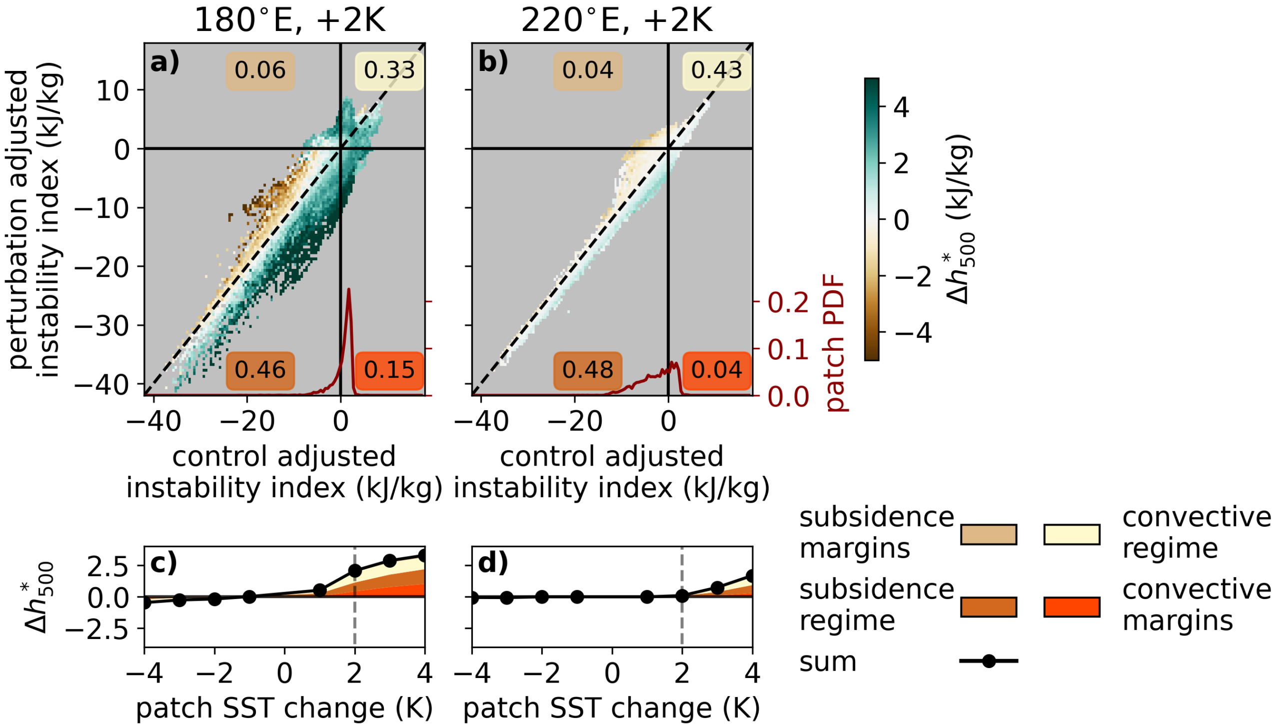

Figure S7. As for Figure 3e-h in the main text, but here showing Δh^*_{500} conditioned on the instability indices. (a) and (b): Δh^*_{500} binned by control (x-axis) and perturbation instability indices (y-axis). (c) and (d): Integrated contributions of the four quadrants (colors) to tropical-mean Δh^*_{500} (black line).

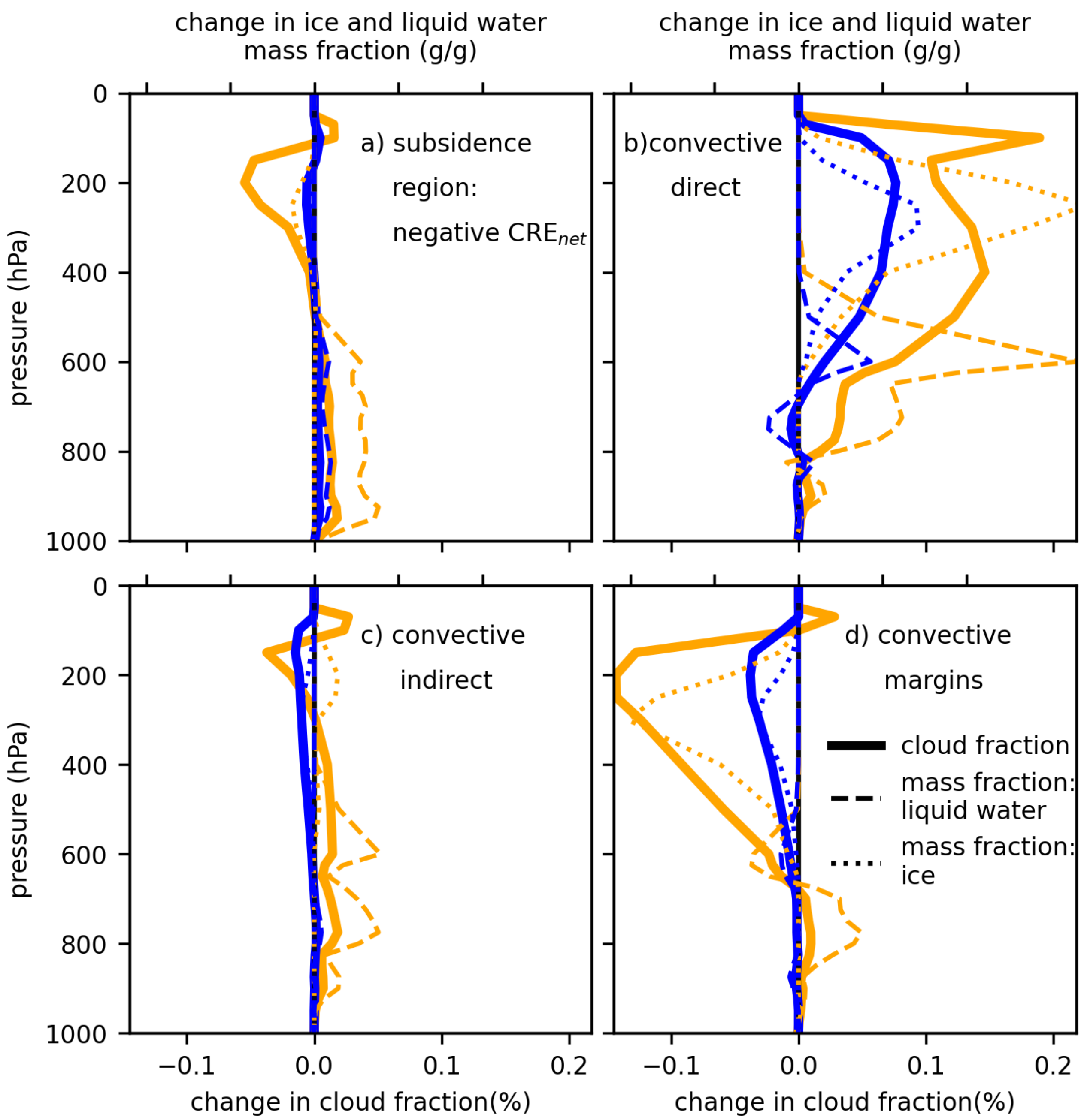

Figure S8. Changes in cloud fraction (bottom x-axes, solid lines) and mass fraction of cloud liquid water and ice (top x-axes, dashed and dotted lines, respectively) averaged over different regimes between the control and +2K simulations for the 180°E (orange) and 220°E (blue) patches. Regimes are: (a) subsidence regime where the $\Delta\mathrm{CRE}_{net} < 0$; (b) convective regime which are directly warmed (i.e. within the patch, as defined by gridpoints with an SST change of greater than +0.4 K in the +4 K warming simulation); (c) convective regime which are not directly warmed (outwith the patch); and (d) convective margins. Note that (a) is a subset of the subsidence regime and (b) and (c) are subsets of the convective regime as defined in the main text.

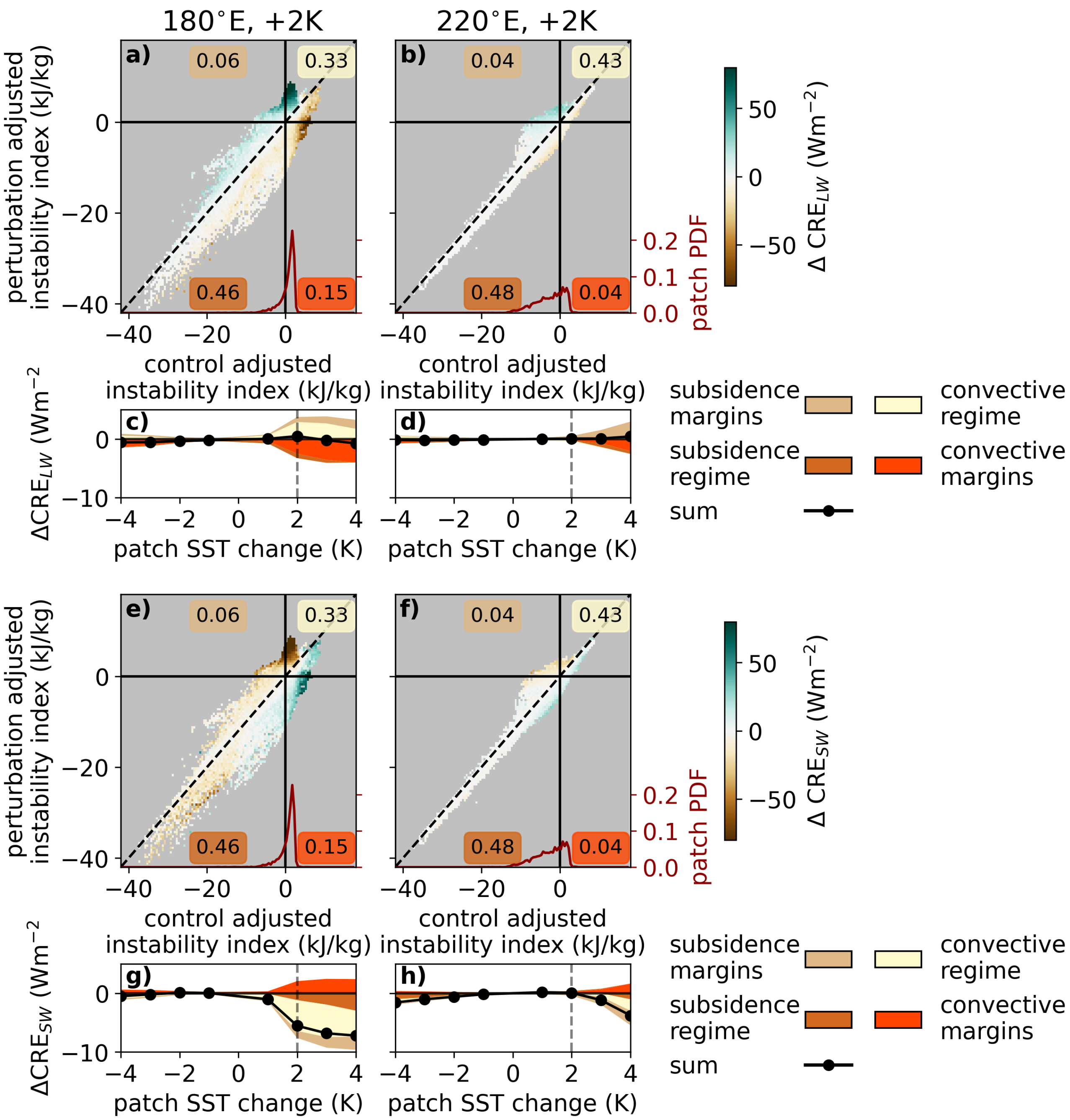

Figure S9. As for Figure 3e-h, but here showing changes in: (a)-(d) longwave CRE; and (e)-(g) shortwave CRE.

References

Holloway, C. E., & Neelin, J. D. (2009). Moisture vertical structure, column water vapor, and tropical deep convection. *Journal of the Atmospheric Sciences*, *66*(6), 1665 - 1683. doi: 10.1175/2008JAS2806.1

Singh, M. S., & O'Gorman, P. A. (2013). Influence of entrainment on the thermal stratification in simulations of radiative-convective equilibrium. *Geophysical Research Letters*, *40*(16). doi: https://doi.org/10.1002/grl.50796